**Transmission Loss Predictions for Dissipative Silencers of**

**Arbitrary Cross-Section in the Presence of Mean Flow**

Ray Kirby

Department of Mechanical Engineering, Brunel University,

Uxbridge, Middlesex, UB8 3PH, UK.

**Abstract**

A numerical technique is developed for the analysis of dissipative silencers of arbitrary, but axially uniform, cross section. Mean gas flow is included in a central airway which is separated from a bulk reacting porous material by a concentric perforate screen. The analysis begins by employing the finite element method to extract the eigenvalues and associated eigenvectors for a silencer of infinite length. Point collocation is then used to match the expanded acoustic pressure and velocity fields in the silencer chamber to those in the inlet and outlet pipes. Transmission loss predictions are compared with experimental measurements taken for two automotive dissipative silencers with elliptical cross sections. Good agreement between prediction and experiment is observed both without mean flow and for a mean flow Mach number of 0.15. It is demonstrated also that the technique presented offers a considerable reduction in computational expenditure when compared to a three dimensional finite element analysis.

## I.     INTRODUCTION

Dissipative silencers are effective for attenuating broad-band noise and are commonly deployed in automotive exhaust and HVAC systems.  A dissipative silencer often takes on a complex geometrical shape, for example in an automotive exhaust system elliptic cross-sections are common.   Modelling complex silencer geometries presents a considerable challenge, especially if one assumes the porous material to be bulk reacting.   Inevitably, numerical techniques have found favour for modelling irregular geometries and for dissipative silencers the finite element method (FEM) is used widely.  A general application of the FEM to dissipative silencer design was presented by Peat and Rathi,[1] who reported transmission loss predictions for two axisymmetric exhaust silencers, both with and without mean flow in the central airway.  The analysis of Peat and Rathi is capable of modelling fully arbitrary silencer geometries, although, in general, this requires the use of a three dimensional finite element mesh[2].  Most silencer geometries are not, however, always of a fully arbitrary shape; in fact, most dissipative silencers usually contain an axially uniform cross section.  For such a silencer it is desirable to take advantage of the uniform geometry and to avoid the significant CPU expenditure associated with a three dimensional finite element model.  One possible solution is to apply the so-called point collocation technique suggested by Astley *et al*.[3] This method is versatile enough to cope with an arbitrary cross-section but also promises to economise on CPU expenditure when compared to the method of Peat and Rathi[1].

The model reported here examines a "straight-through" dissipative silencer containing an axially uniform, but arbitrarily shaped, cross section.  The model includes mean flow in the central airway and also a perforated screen, separating the porous material from the central airway, since this has been shown also to influence silencer performance.[4]  A uniform

silencer facilitates the reduction of the problem from three to two dimensions and in the process potentially reduces CPU expenditure. Thus, the silencer chamber studied here is assumed first to be infinite in length and an eigenvalue analysis is performed. Subsequently the silencer transmission loss is computed by matching the expanded acoustic pressure and velocity fields at the entry/exit planes of the silencer chamber.

The relative simplicity of an eigenvalue analysis, particularly when compared to a three-dimensional approach, has meant that computing modal attenuation rates for dissipative silencers has proved popular, although very few studies progress to calculating silencer transmission loss. For example, Astley and Cummings[5] use the FEM to compute modal attenuation rates in dissipative silencers of rectangular cross-section, adding the effects of mean flow in the central airway. The method of Astley and Cummings was later applied to automotive silencer design by Rathi,[6] who obtained modal attenuation rates for silencers of an elliptic cross-section. Both studies do, however, omit the effects of a perforate and, more importantly, neither progress to predicting the silencer transmission loss. A number of alternative numerical eigenvalue formulations have also been sought for elliptical cross-sections, examples include the Rayleigh Ritz approach of Cummings[7] and the point matching technique of Glav[8]. These alternative formulations do, however, compromise, to some extent, the versatility and robustness of the FEM; the analysis of Cummings is restricted to the fundamental mode only, the method of Glav is very sensitive to silencer geometry and the collocation grid chosen. Moreover, Glav omits both mean flow and a perforate whilst Cummings omits a perforate, and neither study progresses to computing silencer transmission loss.

To predict silencer transmission loss, after first performing an eigenvalue analysis one begins by expressing the acoustic pressure and velocity fields either side of a discontinuity (the inlet and outlet planes in a uniform straight through silencer) as a modal expansion in which only the modal amplitudes are unknown. These are then determined by matching acoustic pressure and normal velocity across each discontinuity. This approach is commonly known as mode matching and has been applied successfully to duct acoustics problems, for example, Åbom[9] implemented an analytic mode matching technique when modelling a reactive exhaust silencer. In general, the method does, however, depend upon finding a transfer matrix $\mathbf{T}$ for the silencer, whose elements $t_{ij}$ decay rapidly with increasing $i, j$. Without this property the solution to the truncated system of matching conditions may bear little resemblance to the solution of the physical problem. The decay of elements $t_{ij}$ largely depends upon the weighting function chosen for the matching scheme. Åbom[9] studied a problem in which the underlying eigen-sub-system is Sturm-Liouville, thus, if one chooses the modal eigenfunctions as weighting functions, modal orthogonality guarantees rapid decay of elements $t_{ij}$. The underlying eigen-sub-system for a dissipative silencer is, however, non Sturm-Liouville and choosing the modal eigenfunctions as weighting functions does not necessarily guarantee a convergent system of equations for a general class of problem. This problem may be addressed by substituting a suitable orthogonality relation which, in effect, restores modal orthogonality. Such an approach was adopted by Glav,[10] who successfully used an orthogonality relation to apply mode matching to a dissipative silencer of arbitrary cross section. To arrive at a transfer matrix Glav utilises an appropriate orthogonality relation which, crucially, is valid only for zero mean flow. To extend the approach of Glav to include mean flow would require the solution of a system of equations in which the chosen weighting function is not orthogonal. Of course the system of equations would remain tractable however convergence to a solution characteristic of the physical problem may not

necessarily be achieved. This behaviour is apparent in the results of Cummings and Chang[11] in which good agreement between prediction and experiment is observed, but only under certain conditions, in this case at higher frequencies. At lower frequencies, when mean flow is present, predictions do not tend towards zero transmission loss, as one would expect. It is possible that this behaviour is caused by the absence of an orthogonality relation in the analysis of Cummings and Chang[11] when mean flow is present, and so the subsequent solution bears little resemblance to the physical problem. In the absence of a suitable orthogonality relation for the present class of problem, caution is therefore exercised and an alternative method is investigated.

A straightforward alternative to analytic mode matching is to use a numerical matching technique. The method of point collocation, implemented by Astley et al.[3] in the study of air-conditioning ducts, appears well suited to automotive silencer design. The technique involves equating velocity and pressure fields at discrete points, or nodal locations, on the cross section of the silencer, rather than integrating over the whole section as is the case when matching analytically. Naturally, matching numerically cannot be expected to be as accurate as matching analytically, however, with a suitable choice of collocation points Kirby and Lawrie[12] demonstrated that, for a rectangular duct lined on opposite walls, excellent agreement with analytic mode matching predictions is possible. Although the study of Kirby and Lawrie omitted mean flow, their results do appear to vindicate the application of point collocation to the current problem. Of course, when implementing point collocation it is convenient first to perform an eigenvalue analysis using the FEM. The collocation points, over which pressure and velocity are matched, may then be chosen at any location over the transverse cross section, although the number of collocation points must not exceed the number of nodes in the original FE mesh. Thus, the analysis presented here first implements

a finite element eigenvalue analysis, based on the method of Astley and Cummings[5] (with the addition of a perforated screen), and then implements a numerical point collocation matching scheme. Predictions are compared with experimental measurements taken for dissipative exhaust silencers with elliptical cross sections.

## II.    GOVERNING EQUATIONS

The dissipative silencer consists of a concentric perforated tube surrounded by an (isotropic) porous material of arbitrary cross-section (see Fig. 1). The silencer chamber, which has a length $L$, is assumed to be uniform along its length, the outer walls of which are assumed to be rigid and impervious. The inlet and outlet pipes (regions $R_1$ and $R_4$) are identical, each having a circular cross section with rigid, impervious, walls.

Prior to matching acoustic pressure and velocity at each axial discontinuity, an eigenvalue analysis is required, both for the silencer chamber and for the inlet/outlet pipes. Finding the eigenvalues and associated eigenvectors for the inlet/outlet pipes is straightforward so listed below is the eigenvalue analysis for the chamber only.

### A.  Governing equations for the silencer chamber.

The acoustic wave equation in region $R_2$ is given by

$$\frac{1}{c_0^2}\frac{D^2 p_2'}{D t^2} - \nabla^2 p_2' = 0,$$

(1)

where $c_0$ is the isentropic speed of sound, $p'$ is the acoustic pressure and $t$ is time. For regions 2 and 3 a coupled modal solution for an axial wavenumber $\lambda$ is sought; thus the sound pressure in region 2 is expanded in the form

$$p'_2(x, y, z; t) = p_2(y, z)\, e^{i(\omega t - k_0 \lambda x)} \,, \tag{2}$$

where $k_0 \ (= \omega/c_0)$ is the wavenumber in region $R_2$, $i = \sqrt{-1}$ and $\omega$ is the radian frequency. Substituting the assumed form for $p'_2$ into the governing wave equation gives

$$\nabla^2_{yz} p_2 + k_0^2 [1 - \lambda M]^2 p_2 - k_0^2 \lambda^2 p_2 = 0 \,, \tag{3}$$

where $M$ is the mean flow Mach number in region $R_2$ and $\nabla_{yz}$ denotes a two dimensional form of the Laplacian operator ($y, z$ plane).

Similarly for region $R_3$, if the sound pressure is expanded in the form

$$p'_3(x, y, z; t) = p_3(y, z)\, e^{i(\omega t - k_0 \lambda x)} \,, \tag{4}$$

the wave equation may be written as

$$\nabla^2_{yz} p_3 - \left(\Gamma^2 + k_0^2 \lambda^2\right) p_3 = 0 \,, \tag{5}$$

provided mean flow in this region is assumed to be negligible and $\Gamma$ is the propagation constant of the porous material.

The appropriate boundary conditions which link together regions $R_2$ and $R_3$ are continuity of normal particle displacement and a pressure condition which takes into account the presence of the perforate. It is convenient to write each boundary condition in terms of the acoustic particle velocity; thus for continuity of displacement

$$\mathbf{u_2} \cdot \mathbf{n_2} = -(1 - M\lambda)\mathbf{u_3} \cdot \mathbf{n_3} \qquad \text{on } S_c, \tag{6}$$

and for pressure

$$p_{c_3} - p_{c_2} = \rho_0 c_0 \zeta \mathbf{u_3} \cdot \mathbf{n_3} \qquad \text{on } S_c. \tag{7}$$

Here, $\mathbf{u}$ is the acoustic velocity vector, $\mathbf{n}$ the outward unit normal vector, and $p_c$ is the sound pressure on boundary $S_c$ (the perforate) either in region $R_2$ or region $R_3$. The (dimensionless) acoustic impedance of the perforate is denoted by $\zeta$ and $\rho_0$ is the mean fluid density in region $R_2$. The assumption of an infinitesimally thin perforate is implicit in Eq. (7) and is valid because the thickness of the perforate is typically small when compared to the overall dimensions of the silencer. Finally, for the outer wall of the silencer chamber (surface $S_3$), the normal pressure gradient is zero; thus

$$\nabla_{yz} p_3 \cdot \mathbf{n_3} = 0 \qquad \text{on } S_3. \tag{8}$$

## B. Finite element discretization and derivation of eigenequation.

The acoustic pressure in the chamber is approximated by a trial solution of the form

$$p_2(y, z) = \sum_{J=1}^{N_2} \psi_{2_J}(y, z) p_{2_J} \quad \text{and} \quad p_3(y, z) = \sum_{J=1}^{N_3} \psi_{3_J}(y, z) p_{3_J} \tag{9a, b}$$

for regions $R_2$ and $R_3$ respectively. Here $\psi_J(y,z)$ is a global basis function, $p_J$ is the value

of $p(y,z)$ at node $J$, and $N_2$ and $N_3$ are the number of nodes in regions $R_2$ and $R_3$,

respectively. To arrive at the governing eigenequation the weak Galerkin method is adopted

and so for region $R_2$ the wave equation may be re-written as

$$\int_{R_2} \left[ \nabla_{yz}^2 p_2 + k_0^2 [1 - \lambda M]^2 p_2 - k_0^2 \lambda^2 p_2 \right] \psi_I \, dydz = 0, \quad \text{for nodes } I = 1, \ldots, N_2. \tag{10}$$

Applying Green's theorem to equation (10) yields

$$\int_{R_2} \left[ \nabla_{yz} \psi_I \nabla_{yz} p_2 + k_0^2 [1 - \lambda M]^2 \psi_I p_2 - k_0^2 \lambda^2 \psi_I p_2 \right] dydz = \int_{S_{C_2}} \psi_I \nabla p_2 \cdot \mathbf{n_2} \, ds, \tag{11}$$

where $S_{c_2}$ denotes the surface of the perforated tube which lies in region $R_2$ and $s$ is an

element length on surface $S_c$. Substituting the assumed trial solution for $p_2$ [Eq. (9a)] into

Eq. (11) gives

$$\left\{ \int_{R_2} \left[ \nabla_{yz} \psi_I \nabla_{yz} \psi_J + k_0^2 \left( \lambda^2 - [1 - \lambda M]^2 \right) \psi_I \psi_J \right] dydz \right\} \{\mathbf{p_2}\} = \int_{S_{C_2}} \psi_I \nabla_{yz} p_2 \cdot \mathbf{n_2} \, ds. \tag{12}$$

Similarly, the weak Galerkin method allows the wave equation in region $R_3$ to be written as

$$\left\{ \int_{R_3} \left[ \nabla_{yz} \psi_I \nabla_{yz} \psi_J + \left( \Gamma^2 + k_0^2 \lambda^2 \right) \psi_I \psi_J \right] dydz \right\} \{\mathbf{p_3}\} = \int_{S_{C_3}} \psi_I \nabla_{yz} p_3 \cdot \mathbf{n_3} \, ds, \tag{13}$$

after utilising the pressure boundary condition on surface $S_3$ [Eq. (8)]. Here $S_{c_3}$ denotes the surface of the perforated tube which lies in region 3.

The final eigenequation for the chamber is obtained by using the boundary conditions on the surface $S_c$ to couple together Eqs. (12) and (13). To facilitate the introduction of the pressure and displacement boundary conditions it is necessary first to write the linearised Euler equation, which for regions $R_2$ and $R_3$ gives

$$\nabla_{yz} p_2 = -i\rho_0\omega(1 - M\lambda)\mathbf{u_2} \text{ and } \nabla_{yz} p_3 = -i\rho(\omega)\omega\mathbf{u_3}, \quad \text{(14a, b)}$$

where $\rho(\omega)$ is the equivalent complex density of the porous material (see Allard and Champoux[13]). By substituting Eq. (14a) into the right hand side of Eq. (12), the displacement boundary condition [Eq. (6)] may be introduced, giving

$$\left\{\int_{R_2} \left[\nabla_{yz}\psi_I \nabla_{yz}\psi_J + k_0^2\left(\lambda^2 - [1 - \lambda M]^2\right)\psi_I\psi_J\right]dydz\right\}\{\mathbf{p_2}\} = i\rho_0\omega[1 - M\lambda]^2 \int_{S_{C_2}} \psi_I\mathbf{u_3}\cdot\mathbf{n_3}ds. \quad \text{(15)}$$

For region 3, substitution of Eq. (14b) into the right hand side of Eq. (13) yields

$$\left\{\int_{R_3} \left[\nabla_{yz}\psi_I \nabla_{yz}\psi_J + \left(\Gamma^2 + k_0^2\lambda^2\right)\psi_I\psi_J\right]dydz\right\}\{\mathbf{p_3}\} = -i\rho(\omega)\omega \int_{S_{C_3}} \psi_I\mathbf{u_3}\cdot\mathbf{n_3}ds. \quad \text{(16)}$$

The pressure boundary condition [Eq. (7)] may now be substituted into the right-hand side of both Eqs. (15) and (16) to yield two equations which may then be combined to give a single eigenequation of the form

11

$$\left\{\int_{R_2}\left[\nabla_{yz}\psi_I\nabla_{yz}\psi_J+k_0^2\left(\lambda^2-[1-\lambda M]^2\right)\psi_I\psi_J\right]dydz\right\}\{\mathbf{p_2}\}+$$

$$\left\{\int_{R_3}\left[\nabla_{yz}\psi_I\nabla_{yz}\psi_J+\left(\Gamma^2+k_0^2\lambda^2\right)\psi_I\psi_J\right]dydz\right\}\{\mathbf{p_3}\}$$

$$-i\frac{k_0}{\zeta}[1-M\lambda]^2\left\{\int_{S_{C_2}}\psi_I\psi_J ds\right\}\{\mathbf{p_{C_3}}-\mathbf{p_{C_2}}\}+i\frac{k_0}{\zeta}\frac{\rho(\omega)}{\rho_0}\left\{\int_{S_{C_3}}\psi_I\psi_J ds\right\}\{\mathbf{p_{C_3}}-\mathbf{p_{C_2}}\}=0.\tag{17}$$

Equation (17) constitutes a second order eigenvalue problem in $\lambda$. It is noticeable that the order of this eigenequation has been reduced by 2 when compared to a similar study by Astley and Cummings[5], who omitted the perforate. Re-writing equation (17) in matrix form, and re-arranging into ascending orders of $\lambda$, gives

$$\left[[\mathbf{A}]+\lambda[\mathbf{B}]+\lambda^2[\mathbf{C}]\right]\{\mathbf{p}\}=\{\mathbf{0}\},\tag{18}$$

where $\mathbf{p}$ is a vector accommodating the pressure in both regions 2 and 3. The matrices $[\mathbf{A}]$, $[\mathbf{B}]$ and $[\mathbf{C}]$ are given by

$$[\mathbf{A}]\{\mathbf{p}\}=[\mathbf{K_2}]\{\mathbf{p_2}\}-k_0^2[\mathbf{M_2}]\{\mathbf{p_2}\}+[\mathbf{K_3}]\{\mathbf{p_3}\}+\Gamma^2[\mathbf{M_3}]\{\mathbf{p_3}\}+\frac{ik_0}{\zeta}[\mathbf{M_{C_2}}]\{\mathbf{p_{C_2}}\}$$

$$-\frac{ik_0}{\zeta}\frac{\rho(\omega)}{\rho_0}[\mathbf{M_{C_3}}]\{\mathbf{p_{C_2}}\}-\frac{ik_0}{\zeta}[\mathbf{M_{C_2}}]\{\mathbf{p_{C_3}}\}+\frac{ik_0}{\zeta}\frac{\rho(\omega)}{\rho_0}[\mathbf{M_{C_3}}]\{\mathbf{p_{C_3}}\},\tag{19}$$

$$[\mathbf{B}]\{\mathbf{p}\}=2Mk_0^2[\mathbf{M_2}]\{\mathbf{p_2}\}-\frac{2ik_0M}{\zeta}[\mathbf{M_{C_2}}]\{\mathbf{p_{C_2}}\}+\frac{2ik_0M}{\zeta}[\mathbf{M_{C_2}}]\{\mathbf{p_{C_3}}\},\tag{20}$$

$$[\mathbf{C}]\{\mathbf{p}\}=k_0^2\left(1-M^2\right)[\mathbf{M_2}]\{\mathbf{p_2}\}+k_0^2[\mathbf{M_3}]\{\mathbf{p_3}\}+\frac{ik_0M^2}{\zeta}[\mathbf{M_{C_2}}]\{\mathbf{p_{C_2}}\}-\frac{ik_0M^2}{\zeta}[\mathbf{M_{C_2}}]\{\mathbf{p_{C_3}}\},\tag{21}$$

and

$$[\mathbf{K_2}]_{I,J} = \int\limits_{R_2} \nabla_{yz}\psi_I \nabla_{yz}\psi_J \, dydz \tag{22a}$$

$$[\mathbf{K_3}]_{I,J} = \int\limits_{R_3} \nabla_{yz}\psi_I \nabla_{yz}\psi_J \, dydz \tag{22b}$$

$$[\mathbf{M_2}]_{I,J} = \int\limits_{R_2} \psi_I \psi_J \, dydz \tag{22c}$$

$$[\mathbf{M_3}]_{I,J} = \int\limits_{R_3} \psi_I \psi_J \, dydz \tag{22d}$$

$$[\mathbf{M_{C_2}}]_{I,J} = \int\limits_{S_{C_2}} \psi_I \psi_J \, ds \tag{22e}$$

$$[\mathbf{M_{C_3}}]_{I,J} = \int\limits_{S_{C_3}} \psi_I \psi_J \, ds. \tag{22f}$$

Finally, the problem may be solved for $\lambda$ by re-writing Eq. (18) as

$$\begin{bmatrix} \mathbf{0} & \mathbf{I} \\ -[\mathbf{C}]^{-1}[\mathbf{A}] & -[\mathbf{C}]^{-1}[\mathbf{B}] \end{bmatrix} \begin{Bmatrix} \mathbf{p} \\ \lambda\mathbf{p} \end{Bmatrix} = \lambda \begin{Bmatrix} \mathbf{p} \\ \lambda\mathbf{p} \end{Bmatrix}, \tag{23}$$

where $\mathbf{I}$ is an identity matrix.

## C. Numerical matching of sound fields.

Acoustic pressure and normal particle velocity are to be matched at collocation points on the silencer inlet and exit planes, thus at plane A (see Fig. 1),

13

$$\mathbf{p}_1'(0, y, z) = \mathbf{p}_2'(0, y, z), \qquad (y, z) \in R_2 \,(\text{or } R_1), \tag{24a}$$

$$\mathbf{u}_{x_1}'(0, y, z) = \mathbf{u}_{x_2}'(0, y, z), \qquad (y, z) \in R_2 \,(\text{or } R_1), \tag{24b}$$

$$0 = \mathbf{u}_{x_3}'(0, y, z), \qquad (y, z) \in R_3, \tag{24c}$$

and for plane B,

$$\mathbf{p}_2'(L, y, z) = \mathbf{p}_4'(L, y, z), \qquad (y, z) \in R_2 \,(\text{or } R_4), \tag{25a}$$

$$\mathbf{u}_{x_2}'(L, y, z) = \mathbf{u}_{x_4}'(L, y, z), \qquad (y, z) \in R_2 \,(\text{or } R_4), \tag{25b}$$

$$\mathbf{u}_{x_3}'(L, y, z) = 0, \qquad (y, z) \in R_3, \tag{25c}$$

where $\mathbf{u}_x'$ is the axial particle velocity. The acoustic pressure and velocity on either side of a discontinuity are now written in terms of a modal expansion, containing both incident and reflected waves. Prior to solving the problem, each modal expansion must be truncated appropriately. Here the modal sum is truncated at the number of collocation points chosen for an individual region. Thus, in region $R_1$, if $N_1$ collocation points are chosen, the sound pressure may be expressed as

$$\mathbf{p}_1'(x, y, z) = P_{i_1}^1 \mathbf{\Phi}_i^1 e^{-ik_0 x/(1+M)} + \sum_{n=1}^{N_1} P_{r_1}^n \mathbf{\Phi}_r^n e^{-ik_0 \lambda_{r_1}^n x}, \qquad (y, z) \in R_1 \,(\text{or } R_2), \tag{26}$$

where $P_{i_1}^1$ is the (known) modal amplitude in the inlet pipe, which is assumed here to contain a plane incident wave only (hence $\mathbf{\Phi}_i^1$ is a unit vector of length $N_1$). Here, the unknown reflected modal amplitudes are denoted by $P_{r_1}^n$, the (known) eigenvalues and associated

eigenvectors are denoted $\lambda_{r_1}^n$ and $\mathbf{\Phi}_r^n$ respectively, where $\mathbf{\Phi}_r$ is a vector of length $N_1$. Thus, the number of unknown modal amplitudes $P_{r_1}^n$ is equal to the number of collocation points in region $R_1$. Of course, on applying point collocation it is necessary to map the collocation points in region $R_1$ onto those in region $R_2$, and so $N_1 = N_2$. Similarly for region 4,

$$\mathbf{p}_4'(x, y, z) = \sum_{n=1}^{N_4} P_{i_4}^n \mathbf{\Phi}_i^n e^{-ik_0 \lambda_{i_4}^n x'}, \qquad (y, z) \in R_4 (\text{or } R_2), \qquad (27)$$

assuming the outlet pipe is terminated anechoically downstream of plane B. Again, the collocation points in region $R_4$ should map onto those chosen in region $R_2$, and so $N_2 = N_4$. For the silencer chamber, the overall number of collocation points in regions $R_2$ and $R_3$ are chosen as $N_2 + N_3 = N_C$. Hence the modal expansion of the pressure field in the chamber is given by

$$\mathbf{p}_c'(x, y, z) = \sum_{n=1}^{N_C} P_{i_c}^n \mathbf{\Psi}_{i_c}^n e^{-ik_0 \lambda_{i_c}^n x} + \sum_{n=1}^{N_C} P_{r_c}^n \mathbf{\Psi}_{r_c}^n e^{-ik_0 \lambda_{r_c}^n x}, \qquad (y, z) \in R_2 + R_3, \qquad (28)$$

where $P_{i_c}^n$ and $P_{r_c}^n$ are the unknown modal amplitudes for the chamber. For the silencer chamber, the eigenvalues $\lambda_{i_c}^n$ and $\lambda_{r_c}^n$, and the associated eigenvectors $\mathbf{\Psi}_{i_c}^n$ and $\mathbf{\Psi}_{r_c}^n$ (each of length $N_C$) are obtained on solution of Eq. (23). The modal expansions may now be substituted into Eqs. (24) and (25), and the matching conditions enforced at each individual node making up the transverse mesh, thus

$$\sum_{n=1}^{N_2} P_{r_1}^n \boldsymbol{\Phi}_r^n - \sum_{n=1}^{N_c} P_{i_c}^n \boldsymbol{\Psi}_{i_c}^n - \sum_{n=1}^{N_c} P_{r_c}^n \boldsymbol{\Psi}_{r_c}^n = -P_{i_1}^1 \boldsymbol{\Phi}_i^1, \quad \text{on } R_2, \tag{29a}$$

$$\sum_{n=1}^{N_2} P_{r_1}^n \boldsymbol{\Phi}_r^n \frac{\lambda_{r_1}^n}{\left[1 - \lambda_{r_1}^n M\right]} - \sum_{n=1}^{N_c} P_{i_c}^n \boldsymbol{\Psi}_{i_c}^n \frac{\lambda_{i_c}^n}{\left[1 - \lambda_{i_c}^n M\right]} - \sum_{n=1}^{N_c} P_{r_c}^n \boldsymbol{\Psi}_{r_c}^n \frac{\lambda_{r_c}^n}{\left[1 - \lambda_{r_c}^n M\right]} = -P_{i_1}^1 \boldsymbol{\Phi}_i^1, \quad \text{on } R_2, \tag{29b}$$

$$\sum_{n=1}^{N_c} P_{i_c}^n \boldsymbol{\Psi}_{i_c}^n \lambda_{i_c}^n + \sum_{n=1}^{N_c} P_{r_c}^n \boldsymbol{\Psi}_{r_c}^n \lambda_{r_c}^n = 0, \quad \text{on } R_3, \tag{29c}$$

$$\sum_{n=1}^{N_c} P_{i_c}^n \boldsymbol{\Psi}_{i_c}^n e^{-ik_0 \lambda_{i_c}^n L} + \sum_{n=1}^{N_c} P_{r_c}^n \boldsymbol{\Psi}_{r_c}^n e^{-ik_0 \lambda_{r_c}^n L} - \sum_{n=1}^{N_2} P_{i_4}^n \boldsymbol{\Phi}_i^n = 0, \quad \text{on } R_2, \tag{29d}$$

$$\sum_{n=1}^{N_c} P_{i_c}^n \boldsymbol{\Psi}_{i_c}^n \frac{\lambda_{i_c}^n}{\left[1 - M\lambda_{i_c}^n\right]} e^{-ik_0 \lambda_{i_c}^n L} + \sum_{n=1}^{N_c} P_{r_c}^n \boldsymbol{\Psi}_{r_c}^n \frac{\lambda_{r_c}^n}{\left[1 - M\lambda_{r_c}^n\right]} e^{-ik_0 \lambda_{r_c}^n L} - \sum_{n=1}^{N_2} P_{i_4}^n \frac{\lambda_{i_1}^n}{\left[1 - M\lambda_{i_1}^n\right]} \boldsymbol{\Phi}_i^n = 0, \text{ on } R_2 \tag{29e}$$

$$\sum_{n=1}^{N_c} P_{i_c}^n \boldsymbol{\Psi}_{i_c}^n \lambda_{i_c}^n e^{-ik_0 \lambda_{i_c}^n L} + \sum_{n=1}^{N_c} P_{r_c}^n \boldsymbol{\Psi}_{r_c}^n \lambda_{r_c}^n e^{-ik_0 \lambda_{r_c}^n L} = 0, \quad \text{on } R_3. \tag{29f}$$

This yields $4N_2 + 2N_3$ equations (the collocation points) and $2N_2 + 2N_c$ ($= 4N_2 + 2N_3$) unknown modal amplitudes, after putting $P_{i_1}^1 = 1$. Equations (29a)-(29f) may be solved simultaneously to find the unknown modal amplitudes. Finally the sound transmission loss of the silencer (TL) is given by[11]

$$TL = -20 \log \left| p_{i_4}^1 \right|. \tag{30}$$

## III.    EXPERIMENTAL TESTS

Experimental measurements were performed on two dissipative exhaust silencers, called here silencer A and B.  Each silencer is approximately elliptical in cross section and contains a bulk reacting porous material separated from the central airway by a concentric perforated screen (see Fig. 2).  The chamber dimensions are summarised in Table I (for each silencer the radius $r$ of the perforated tube is 37 mm).

### A.  Silencer Transmission Loss.

The silencer transmission loss was measured using the impulse technique described by Cummings and Chang[11].  This method is appropriate in the absence of an anechoic chamber and is suited also to tests that involve mean fluid flow.  The technique involves sending a short rectangular pulse through the silencer and capturing the transmitted sound pressure.  The process is repeated after a suitable time interval and the transmitted sound pressure successively averaged.  The same procedure is followed after removal of the silencer from the test rig and the transmission loss is computed by taking the logarithmic ratio of the two captured average sound pressure spectra.  A detailed account of the experimental technique is given by the author in a paper on axisymmetric dissipative silencers,[4] although it should be noted here that the impulse technique inevitably incurs frequency limits outside of which experimental measurements are inaccurate.  At low frequencies, below approximately 150 Hz, erroneous measurements are common and these are caused largely by reflections from the outlet test pipe arriving back at the silencer before all the reflections within the silencer have died away.  An upper frequency limit, approximately 1500 Hz here, is caused by a

significant roll-off in the pressure amplitude of the supplied pulse at frequencies above the sampling frequency of 3 kHz.

**B.  Bulk Acoustic Properties of the Porous Materials.**

Fibre glass and basalt wool are commonly used as acoustic absorbents in automotive silencers.  The fibre glass studied here is known commercially in the UK as E glass and has an approximate average fibre diameter of 5-13 μm; the basalt wool studied here has a slightly larger average fibre diameter of  6-18 μm.  The analysis in Sec. II demands a knowledge of the bulk complex density $\rho(\omega)$, and the propagation constant $\Gamma$ for each porous material.  It is convenient here to write $\rho(\omega)$ in terms of the (complex) characteristic impedance ($z_a$), where $\rho(\omega) = z_a \Gamma / i\omega$ (see Allard and Champoux[13]).  The propagation constant and characteristic impedance are specified here by combining the empirical power law approach of Delany and Bazley[14] with theoretical low frequency corrections.  The semi-empirical approach of Kirby and Cummings[15] alleviates the non-physical predictions typically obtained when applying Delany and Bazley power laws at low frequencies.  For the materials studied here, values for $\Gamma$ and $z_a$ were given by Kirby and Cummings as

$$\frac{\Gamma}{k_0} = i\sqrt{\gamma_0 q^2(\omega)} \left\{ \frac{[\ln(1-\Omega)+1+2\Omega]\Omega \ln(1-\Omega)+\Omega^2+3\Omega^3/2+\Omega^4/3}{[\ln(1-\Omega)+\Omega+\Omega^2/2]^2} - \left(\frac{\gamma_0-1}{\gamma_0}\right) Pr - i \frac{\Omega}{2\pi\xi_f q_0^2 s^2(\omega)} \right\}^{\frac{1}{2}},$$
(31)

$$\frac{z_a}{\rho_0 c_0} = \sqrt{\frac{q^2(\omega)}{\gamma_0 \Omega^2}} \left\{ \frac{[\ln(1-\Omega)+1+2\Omega]\Omega \ln(1-\Omega)+\Omega^2+3\Omega^3/2+\Omega^4/3}{[\ln(1-\Omega)+\Omega+\Omega^2/2]^2} + \left(\frac{\gamma_0-1}{\gamma_0}\right) Pr - i \frac{\Omega}{2\pi\xi_f q_0^2 s^2(\omega)} \right\}^{\frac{1}{2}},$$
(32)

18

where $\Omega$ is the porosity of the porous material, $\xi_f$ is a dimensionless frequency parameter

($\xi_f = \rho_0 f / \sigma_b$, where $f$ is frequency and $\sigma_b$ is the flow resistivity of the bulk porous

material), $\gamma_0$ is the ratio of specific heats for air, Pr is the Prandtl number, and $q_0$ is the so-

called steady flow tortuosity. Kirby and Cummings define a "dynamic" tortuosity $q^2(\omega)$ and

shape factor $s^2(\omega)$ as

$$q^2(\omega) = \frac{\left[\left(1+a_3\xi_f^{a_4}\right)\left(1+a_5\xi_f^{a_6}\right)-a_1a_7\xi_f^{(a_2+a_8)}\right]\left[\ln(1-\Omega)+\Omega+\Omega^2/2\right]^2}{\left[\ln(1-\Omega)+1+2\Omega\right]\ln(1-\Omega)+\Omega+3\Omega^2/2+\Omega^3/3}, \tag{33}$$

$$s^2(\omega) = \frac{q^2(\omega)}{2\pi\xi_f q_0^2}\frac{1}{\left[a_1\xi_f^{a_2}\left(1+a_5\xi_f^{a_6}\right)+a_7\xi_f^{a_8}\left(1+a_3\xi_f^{a_4}\right)\right]}, \tag{34}$$

where $a_1....a_8$ are the Delany and Bazley coefficients measured experimentally.[13]  The

material constants measured for E glass and basalt wool are listed in Table II.  Table II also

defines a transition value for $\xi_f$, denoted here $\xi_{f_0}$, below which $q^2(\omega)$ must be set equal to

$q_0^2$ in Eqs. (31) and (32) (see Kirby and Cummings[15]).

## C.  Acoustic Impedance of Perforate Screen.

The perforate screen used in each of the test silencers was constructed by forming a flat plate

with circular perforations into a concentric screen.  The acoustic impedance of a perforated

plate was shown by Kirby and Cummings[16] to increase when backed by a porous material.

They suggested the following semi-empirical relationship for the non-dimensional perforate

impedance $(\zeta)$,

19

$$\zeta = \frac{1}{\sigma}\left[\zeta' - i0.425k_0 d + \frac{0.425 d z_a \Gamma}{\rho_0 c_0}\right],$$

(35)

where $d$ is the diameter of the hole, $\sigma$ is the area porosity of the perforate and $\zeta'$ is the orifice impedance measured experimentally in the absence of a porous backing, and may be written as $\zeta' = \theta + i\chi$, where $\theta$ is the orifice resistance and $\chi$ the orifice reactance. In the presence of mean flow Kirby and Cummings[16] proposed the following empirical relationship

$$\theta = \left(26.16\left[\frac{t}{d}\right]^{-0.169} - 20\right)\frac{u_*}{c_0} - 0.6537 k_0 d + \frac{t}{d}\sqrt{8k_0\nu/c_0},$$

(36)

where $t$ is the thickness of the plate, $\nu$ is the kinematic viscosity of the mean gas flow, and $u_*$ is the friction velocity of the mean gas flow measured on the inner wall of the perforate. The orifice reactance is given by $\chi = ik_0(\delta + t)$, and Kirby and Cummings[16] proposed

$$\frac{\delta}{\delta_0} = 1, \qquad\qquad\qquad\qquad\qquad u_*/ft \le 0.18 d/t,$$

$$\frac{\delta}{\delta_0} = \left(1 + 0.6\frac{t}{d}\right)\exp\left\{-\frac{u_*/ft - 0.18 d/t}{1.8 + t/d}\right\} - 0.6t/d, \qquad u_*/ft > 0.18 d/t,$$

(37)

and $\delta_0 = 0.849d$. When no mean flow is present, $\theta$ and $\chi$ were given by Bauer[17] as

$$\theta = (1 + t/d)\sqrt{8k_0\nu/c_0}, \text{ and } \chi = ik_0(0.25d + t).$$

(38a, b)

## IV. RESULTS AND DISCUSSION

The finite element mesh generated for both silencers A and B (see Table I) consisted of 6 noded triangular (in region $R_2$) and 8 noded quadrilateral (in region $R_3$) isoparametric elements. For both silencers, 24 elements (88 nodes) were used to mesh the chamber, this equates to 35 nodes in region $R_2$ and 53 nodes in region $R_3$. Note that in order to implement the pressure change boundary condition across the perforate [see Eq. (7)] it is necessary to place a node on either side of the perforate and then to apply the boundary condition between these two nodes. Thus, the finite element mesh includes two nodes (with identical geometrical coordinates) at each nodal point along the boundary $S_c$. For the inlet and outlet pipes (regions $R_1$ and $R_4$) a mesh identical to the one in region $R_2$ is used, this facilitates the straightforward application of the point collocation matching technique. The silencer transmission loss is calculated from Eq. (30) after first solving simultaneously Eqs. (29). Transmission loss predictions are compared with experimental measurements in Figs. 3-6, for silencers A and B with mean flow Mach numbers of $M = 0$ and $M = 0.15$. Theoretical predictions for $M = 0$ were obtained by eliminating matrix $[\mathbf{B}]$ from Eq. (23) prior to solution. For each silencer a concentric perforate screen of thickness $t = 1\,\mathrm{mm}$, hole diameter of $d = 3.5\,\mathrm{mm}$ and an open area porosity of $\sigma = 0.263$ was used. When a mean flow Mach number of $M = 0.15$ is present, the friction velocity was measured to be $u_* = 2.56\,\mathrm{m/s}$.

It is evident in Figs. 3-6 that good agreement generally exists between measured and predicted silencer transmission loss. For frequencies below 1 kHz, predictions lie within approximately 2 dB of measured values, although the transmission loss does tend to be over-predicted. Above 1 kHz, a comparison with experiment is generally less successful and

21

differences of up to 6 dB are evident, largely for those measurements taken without mean flow. Larger discrepancies at higher frequencies are, however, likely to be caused by experimental error. Nevertheless, over the frequency range studied here, agreement between prediction and experiment is deemed to be acceptable and is at least comparable in accuracy to studies of dissipative silencers by other authors; see, for example, Cummings and Chang,[11] Astley and Cummings,[3] and Aurégan et al.[18]. Finally, the influence of the perforate is examined in Figs. 7 and 8. Here a number of different values for perforate porosity are examined for silencers A and B with a mean flow Mach number of 0.15. It is evident that, at least for the silencers studied here, a small increase in transmission loss is obtained at low frequencies when the perforate porosity is reduced, however, this is at the expense of a large reduction in transmission loss at higher frequencies.

The computation of silencer transmission loss requires the inversion of three matrices: one of order $N_2$ (the inlet/outlet eigenvalues), one of order $N_c$ (the chamber eigenvalues), and one of order $2(N_2 + N_c)$ (numerical matching). If one assumes a solver speed proportional to $N^3$ then this CPU expenditure is generally higher than for an equivalent analytic matching procedure. However, in the absence of a reliable analytic mode matching scheme when mean flow is present, CPU expenditure compares favourably with the alternative fully three dimensional treatment of Peat and Rathi[1]. For example, the method of Peat and Rathi was applied to silencers A and B (see Table I) by Kirby[2] (after omitting the perforate) and, although generally good agreement between prediction and experiment was observed, the three dimensional mesh required 1497 degrees of freedom for silencer A and 1757 for silencer B. Thus for the silencers studied here point collocation represents a considerable saving in CPU run time, amounting to approximately 99.5% for a solver whose speed is proportional to $N^3$.

The solution of Eq. (23) generates an unordered list of $N_c$ incident and $N_c$ reflected eigenvalues and associated eigenvectors. The imaginary part of the incident and reflected eigenmodes are then sorted into ascending order prior to the application of mode matching. It is noticeable that, on solving Eq. (23) with mean flow present, so-called hydrodynamic modes are not found. This is in contrast to a similar study by Astley and Cummings[5] and is caused by a change in the boundary condition between the airway and the porous material. In the analysis presented here only transverse acoustic particle displacement across the perforate is allowed. More importantly, transverse mean flow effects are suppressed at the perforate that effectively prevents the formation of a fully free shear layer and serves to suppress the generation of hydrodynamic modes. Of course, hydrodynamic modes have long been known to exist when mean flow is present, and they are known to play an important role in the performance of reactive silencers, however, when a porous material is present it is likely that strong damping is provided by the material, and this will serve to reduce significantly the influence of hydrodynamic modes on the sound pressure field. Thus, it is assumed in the analysis presented in Sec. II, and the results presented here, that the acoustic performance of the silencer is dominated by the behaviour of the least attenuated propagating modes and that the effects of hydrodynamic modes may be neglected.

The transmission loss predictions shown in Figs. 3-8 were obtained after first establishing a converged solution, that is, the number of collocation points were increased until the variation in transmission loss was negligible over the frequency range shown. For convenience, the collocation points were chosen to be identical to the nodal locations chosen for the eigenvalue analysis, and so adaptation of the collocation points effectively takes place prior to carrying out the eigenvalue analysis. Of course, so long as no more than $N_c$

23

collocation points are chosen, the collocation points need not be coincident with the nodal locations in the original mesh. Moreover, in principle, it should be possible to reduce the size of the collocation problem by reducing the number of collocation points to less than $N_c$. However, as we do not know the shape of the final sound pressure field prior to numerical matching, the choice of where best to put the collocation points becomes problematic, especially at higher frequencies. The author has found the most reliable and robust approach by choosing collocation points coincident in location with the nodes chosen for the eigenvalue problem and to adapt the eigenvalue mesh only, i.e., to follow a standard finite element adaptive procedure. Thus, for the current problem, matching is carried out over 35 collocation points in region $R_2$, and 53 points in region $R_3$ - collocation points equivalent in number to the number of eigensolutions found in the silencer chamber. Of course, it is widely known that for a finite element eigenvalue analysis one can rely on the accuracy only of about 20% of the eigensolutions found. This does not present a problem here since the sound pressure field at an individual collocation point is expressed as a modal sum [see Eqs. (26)-(28)] and it is likely that, at least for the dissipative silencers studied here, the performance of the silencer is dominated by the least attenuated modes, and these are the modes which are found with the most accuracy using the FEM. For the current problem, approximately 18 least attenuated modes may be deemed to be accurate and this number should be more than sufficient to achieve a convergent sum in Eqs. (26)-(28), assuming that hydrodynamic modes may be neglected. Thus, to solve the problem efficiently one needs sufficient least attenuated modes to represent accurately the sound pressure field at an individual collocation point, but also a sufficient number of points to accommodate the variation in the transverse sound pressure field. For the current problem, 88 collocation points are chosen in the chamber and, to maintain a square matrix and hence a tractable problem, 88 eigenmodes are used in Eq. (28). On solving Eqs. (29) errors will therefore be

present in 80% of the modal amplitudes found, however these are amplitudes of highly attenuated modes and so the effect on the overall silencer performance is negligible.

The transmission loss predictions presented in Figs. 3-8 cover a frequency range restricted by experimental measurements. The technique presented here may, however, be used over a much wider frequency range, provided the finite element mesh is adapted in the normal way. This has been demonstrated by Kirby and Lawrie[12] who successfully applied point collocation to a relatively large HVAC silencer, although mean flow was omitted. Kirby and Lawrie computed the transmission loss for a rectangular duct of cross-sectional dimensions 1.5 m×1.5 m and lined on opposite walls with a bulk reacting material. Excellent agreement between point collocation predictions and an exact analytic solution was reported for frequencies up to 2 kHz, providing supporting evidence as to the accuracy of the current method over a wider frequency range than the one presented here (based on a representative $k_0 a$ value - "$a$" being a representative dimension of the duct).

## IV. CONCLUSIONS

A finite length dissipative silencer of arbitrary, but uniform, cross section has been modelled by combining a finite element eigenvalue analysis with a point collocation matching scheme. The method is computationally efficient when compared to a three-dimensional finite element approach and avoids the question of modal orthogonality. A good correlation between prediction and experiment is observed both with and without mean flow, up to a frequency of 1500 Hz for the silencers studied here, although in principle the method is applicable over a much wider frequency range. Furthermore the flexibility and robustness of the finite element method allows the technique to be applied to any cross sectional dissipative

silencer geometry, such as rectangular air conditioning ducts, and, in principle, to include any number of duct discontinuities.

# REFERENCES

1. K.S. Peat and K.L. Rathi, "A finite element analysis of the convected acoustic wave motion in dissipative silencers," Journal of Sound and Vibration **184**, 529-545 (1995).

2. R. Kirby, " The acoustic modelling of dissipative elements in automotive exhausts," PhD Thesis, University of Hull, UK (1996).

3. R.J. Astley, A. Cummings and N. Sormaz, "A finite element scheme for acoustic propagation in flexible-walled ducts with bulk-reacting liners, and comparison with experiment," Journal of Sound and Vibration **150**, 119-138 (1991).

4. R. Kirby, "Simplified techniques for predicting the transmission loss of a circular dissipative silencer," Journal of Sound and Vibration **243**, 403-426 (2001).

5. R.J. Astley and A. Cummings, "A finite element scheme for attenuation in ducts lined with porous material: comparison with experiment," Journal of Sound and Vibration **116**, 239-263 (1987).

6. K.L. Rathi, "Finite element acoustic analysis of absorption silencers with mean flow," PhD Thesis, Loughborough University, UK (1994).

7. A. Cummings, "A segmented Rayleigh-Ritz method for predicting sound transmission in a dissipative exhaust silencer of arbitrary cross-section," Journal of Sound and Vibration **187**, 23-37 (1995).

8. R. Glav, "The point-matching method on dissipative silencers of arbitrary cross section," Journal of Sound and Vibration **189**, 123-135 (1996).

9. M. Åbom, "Derivation of four-pole parameters including higher order mode effects for expansion chamber mufflers with extended inlet and outlet," Journal of Sound and Vibration **137**, 403-418 (1990).

10. R. Glav, "The transfer matrix for a dissipative silencer of arbitrary cross-section," Journal of Sound and Vibration **236**, 575-594 (2000).

11. A. Cummings and I.-J. Chang, "Sound attenuation of a finite length dissipative flow duct silencer with internal mean flow in the absorbent," Journal of Sound and Vibration **127**, 1-17 (1988).

12. R. Kirby and J.B. Lawrie "Modelling dissipative silencers in HVAC ducts," Proceedings of the Institute of Acoustics Spring Conference, Salford University, Salford, UK., **24**(2) (2002).

13. J.F. Allard and Y. Champoux, "New empirical equations for sound propagation in rigid frame fibrous materials," Journal of the Acoustical Society of America **91**, 3346-3353 (1992).

14. M.E. Delany and E.N. Bazley, "Acoustical properties of fibrous materials," Applied Acoustics **3**, 105-116 (1970).

15. R. Kirby and A. Cummings, "Prediction of the bulk acoustic properties of fibrous materials at low frequencies," Applied Acoustics **56**, 101-125 (1999).

16. R. Kirby and A. Cummings, "The impedance of perforated plates subjected to grazing gas flow and backed by porous media," Journal of Sound and Vibration **217**, 619-636 (1998).

17. A.B. Bauer, "Impedance theory and measurements on porous acoustic liners," Journal of Aircraft **14**, 720-728 (1977).

18. Y. Aurégan, A. Debray and R. Starobinski, "Low frequency sound propagation in a coaxial cylindrical duct: application to sudden area expansions and to dissipative silencers," Journal of Sound and Vibration **243**, 461-473 (2001).

| Table I. Data for test silencers. | | | | |
|---|---|---|---|---|
| Silencer | Major axis ($a$, mm) | Minor axis ($b$, mm) | Length ($L$, mm) | Porous material |
| A | 110 | 60 | 350 | Basalt Wool |
| B | 95 | 50 | 450 | E. Glass |

| Table II. Porous material constants. | | |
|---|---|---|
| Constant | E glass | Basal Wool |
| $a_1$ | 0.2202 | 0.2178 |
| $a_2$ | -0.5850 | -0.6051 |
| $a_3$ | 0.2010 | 0.1281 |
| $a_4$ | -0.5829 | -0.6746 |
| $a_5$ | 0.0954 | 0.0599 |
| $a_6$ | -0.6687 | -0.7664 |
| $a_7$ | 0.1689 | 0.1376 |
| $a_8$ | -0.5707 | -0.6276 |
| $\sigma_b$ (MKS rayl/m) | 30716 | 13813 |
| $\Omega$ | 0.952 | 0.957 |
| $q_0^2$ | 5.49 | 2.91 |
| $\xi_{f_0}$ | 0.005 | 0.0079 |
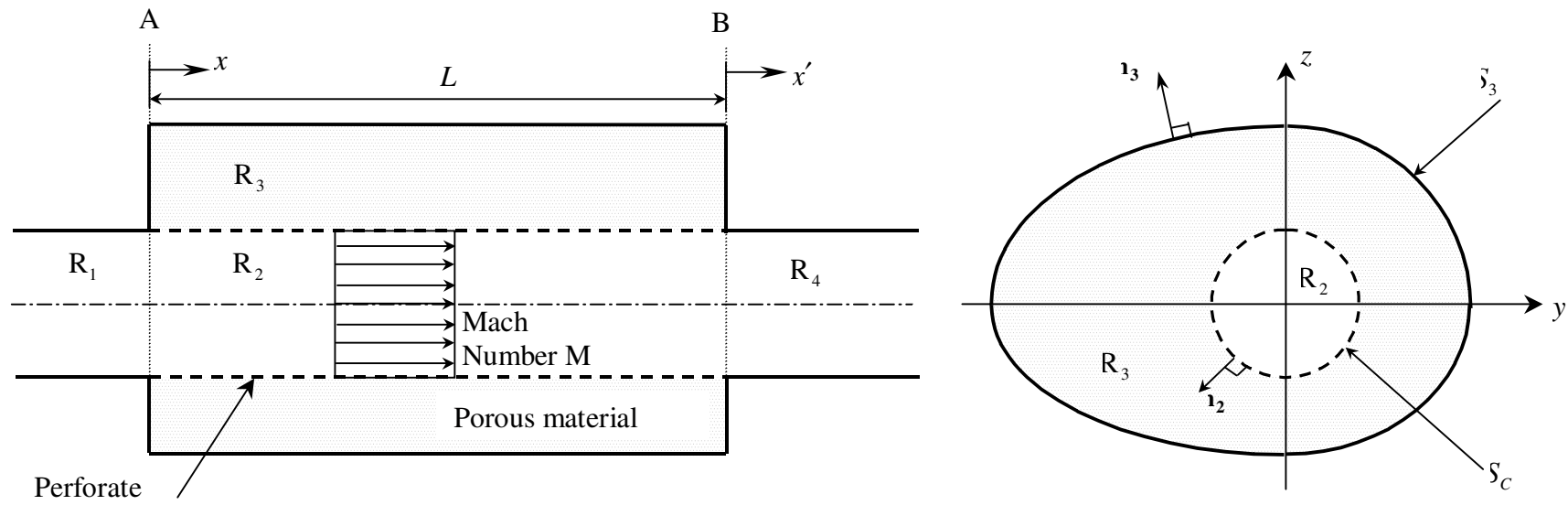
Figure 1. Geometry of silencer.
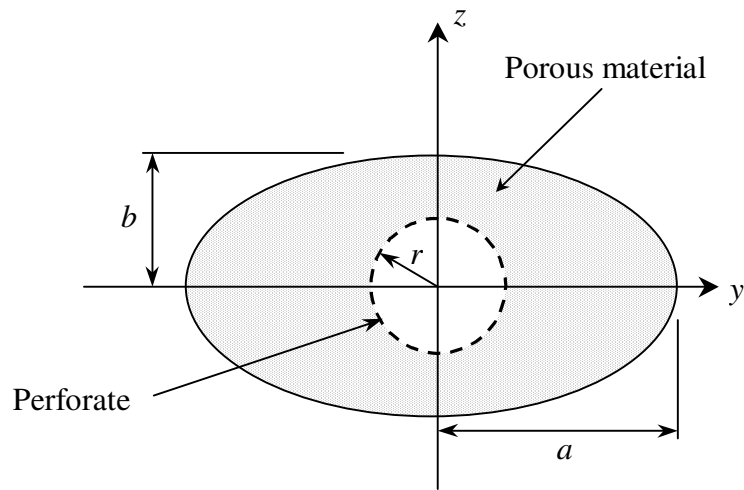
Figure 2. Dimensions of silencer cross section.
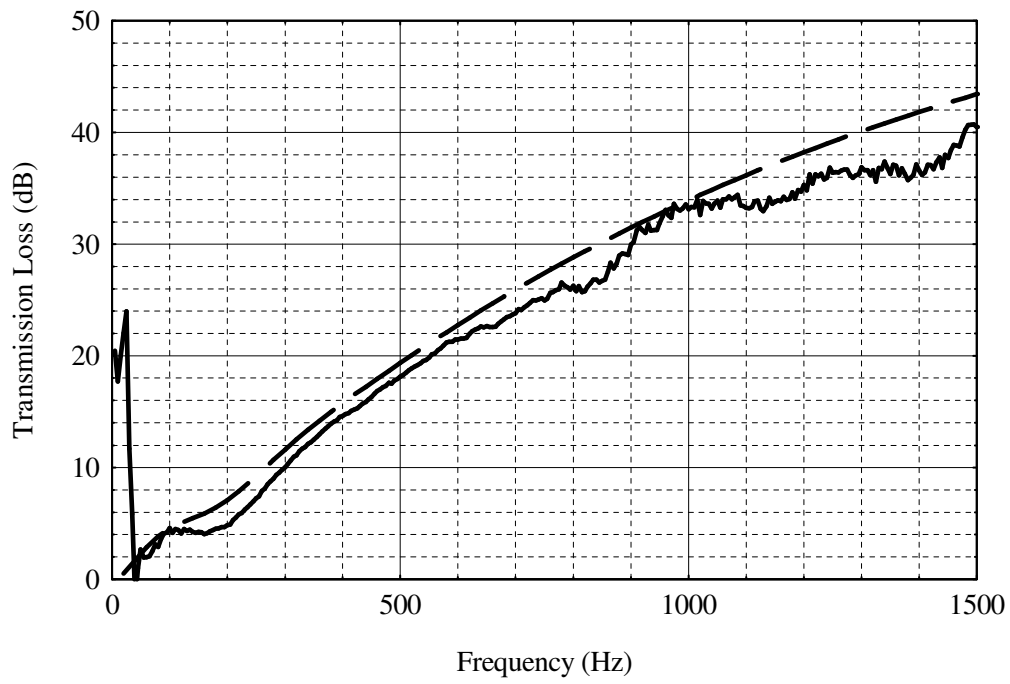
Figure 3. Transmission loss for silencer A with $M = 0$. ———— experimental measurement;
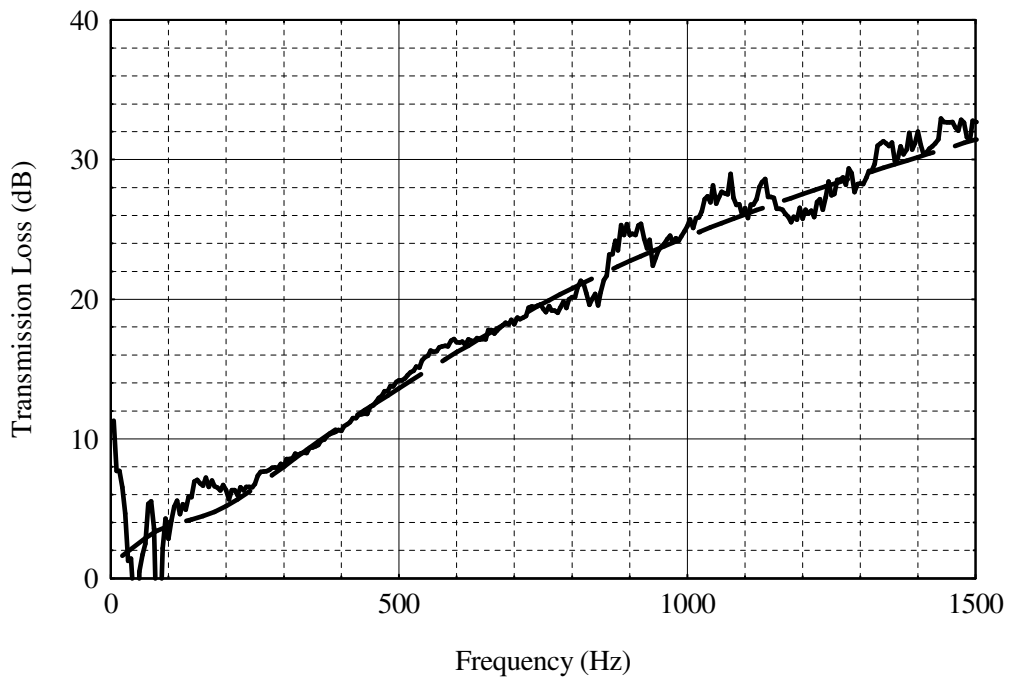
— — — prediction.

Figure 4. Transmission loss for silencer A with $M = 0.15$. ——— experimental
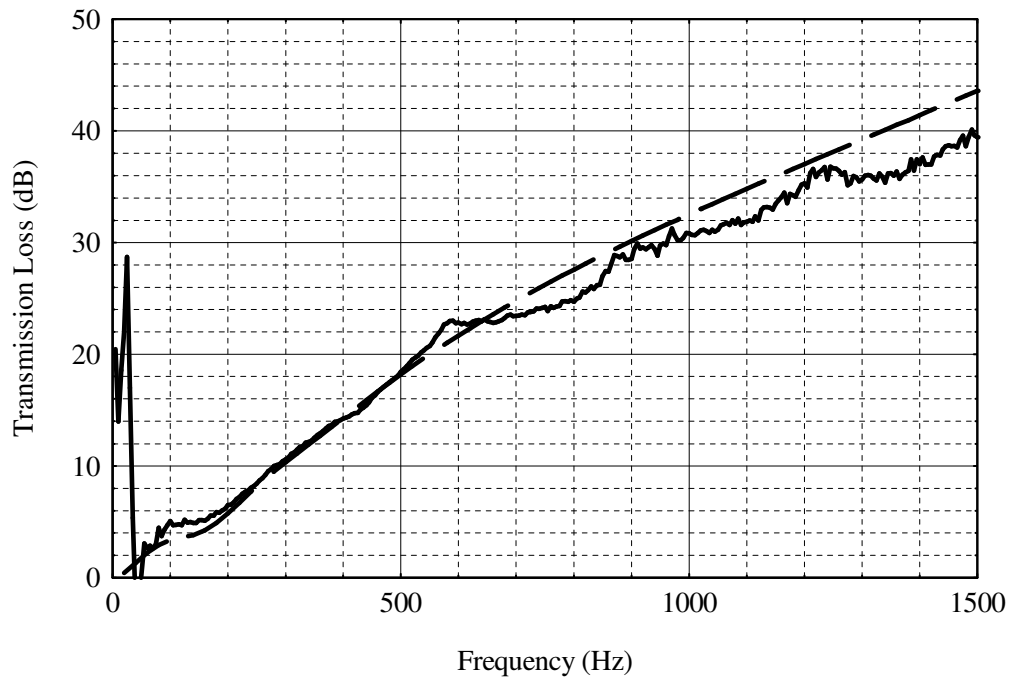
measurement; — — — prediction.

Figure 5.  Transmission loss for silencer B with $M = 0$.  ———— experimental measurement;
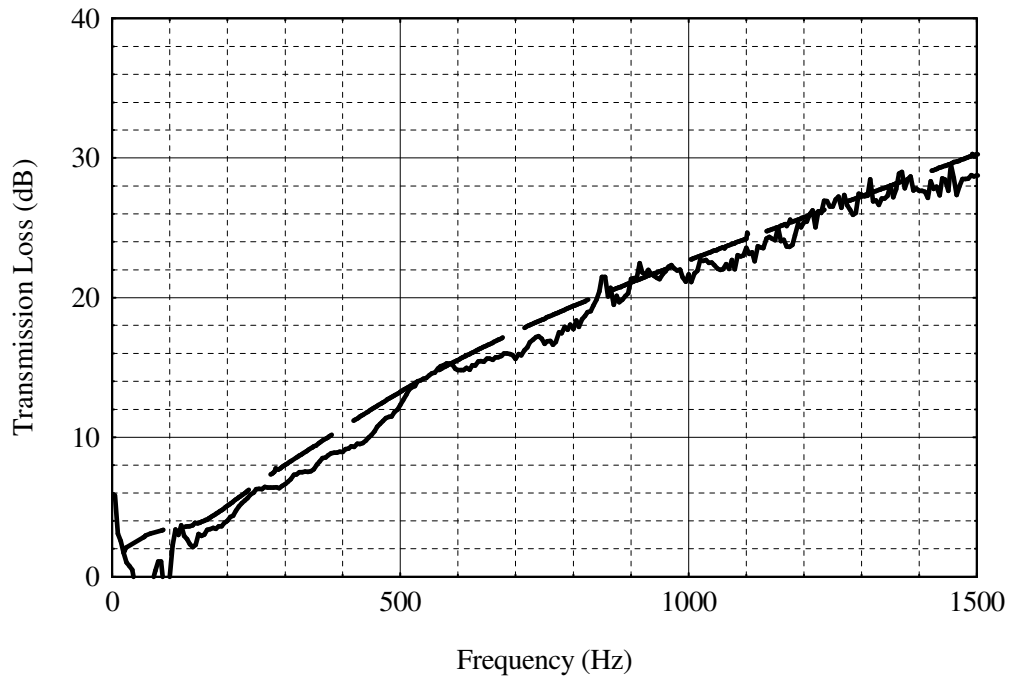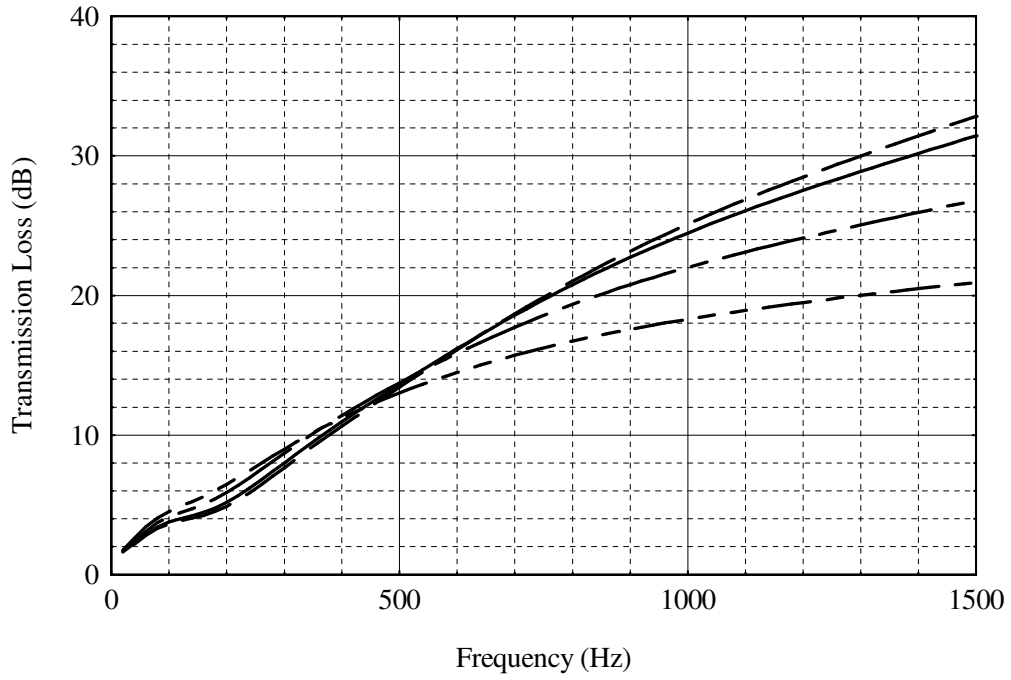
— — —  prediction.

Figure 6. Transmission loss for silencer B with $M = 0.15$. ——— experimental

measurement; — — — prediction.

Figure 7.  Transmission loss predictions for silencer A with $M = 0.15$.  — — — $\sigma = 0.5$;

———— $\sigma = 0.263$; — · — · — $\sigma = 0.1$; — · · — · · — $\sigma = 0.05$.
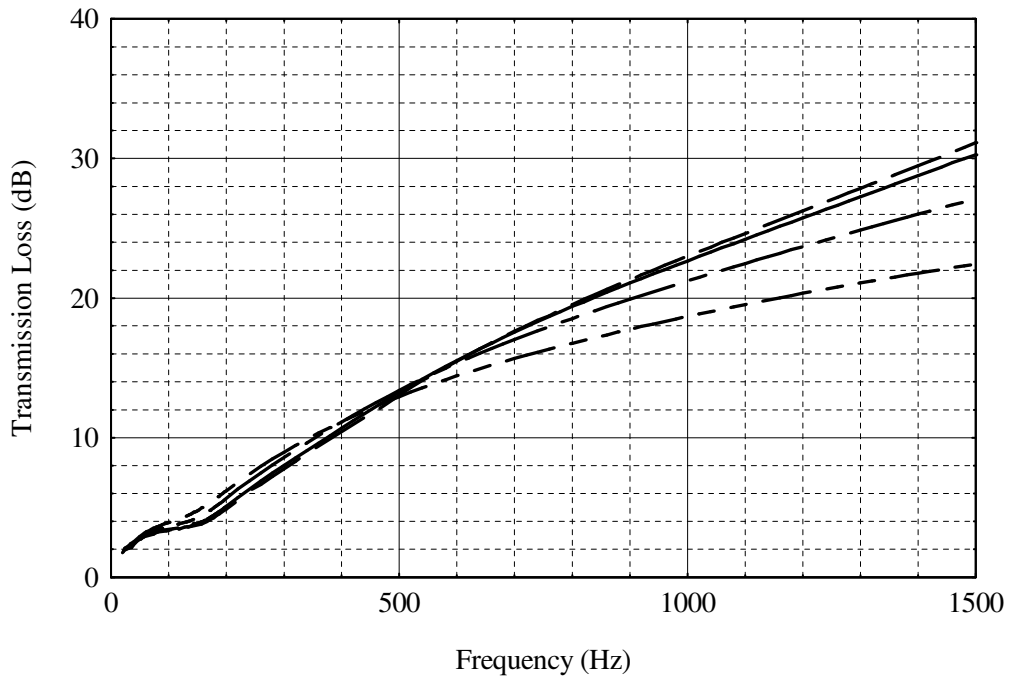
Figure 8. Transmission loss predictions for silencer B with $M = 0.15$. — — — $\sigma = 0.5$; ——— $\sigma = 0.263$; — · — · — $\sigma = 0.1$; — · · — · · — $\sigma = 0.05$.